Magnetothermoacoustics from magnetic nanoparticles by short bursting or frequency chirped alternating magnetic field: A theoretical feasibility analysis

Daqing Piao[a)]
School of Electrical and Computer Engineering, Oklahoma State University, Stillwater, Oklahoma 74078

Rheal A. Towner and Nataliya Smith
Advanced Magnetic Resonance Imaging Center, Oklahoma Medical Research Foundation, Oklahoma City, Oklahoma 73104

Wei R. Chen
Department of Engineering and Physics, University of Central Oklahoma, Edmond, Oklahoma 73034

(Received 13 January 2013; revised 4 April 2013; accepted for publication 22 April 2013; published 13 May 2013)

Purpose: To propose an alternative method of thermoacoustic wave generation based on heating of magnetic nanoparticles (MNPs) using alternating magnetic field (AMF).
Methods: The feasibility of thermoacoustic wave generation from MNPs by applying a short-burst of AMF or a frequency-modulated AMF is theoretically analyzed. As the relaxation of MNPs is strongly dependent upon the amplitude and frequency of AMF, either an amplitude modulated, fixed frequency AMF (termed time-domain AMF) or a frequency modulated, constant amplitude AMF (termed frequency-domain AMF) will result in time-varying heat dissipation from MNPs, which has the potential to generate thermoacoustic waves. Following Rosensweig's model of specific power loss of MNPs in a steady-state AMF, the time-resolved heat dissipations of MNPs of superparamagnetic size when exposed to a short bursting of AMF and/or to a linearly frequency chirped AMF are derived, and the resulted acoustic propagation is presented. Based on experimentally measured temperature-rise characteristics of a superparamagnetic iron-oxide nanoparticle (SPION) matrix in a steady-state AMF of various frequencies, the heat dissipations of the SPION under time-domain and frequency-domain AMF configurations that could have practical utility for thermoacoustic wave generation are estimated.
Results: The initial rates of the temperature-rise of the SPION matrix were measured at an iron-weight concentration of 0.8 mg/ml and an AMF frequency of 88.8 kHz to 1.105 MHz. The measured initial rates of temperature-rise were modeled by Rosensweig's theory, and projected to 10 MHz AMF frequency, at which a 1 μs bursting corresponding to a 1.55 mm axial resolution of acoustic detection could contain 10 complete cycles of AMF oscillation and the power dissipation is approximately 84 times of that at 1 MHz. Exposing the SPION matrix to a 1 μs bursting of AMF at 10 MHz frequency and 100 Oe field intensity would produce a volumetric heat dissipation of 7.7 μJ/cm^3 over the microsecond duration of the AMF burst. If the SPION matrix is exposed to a 1 ms long AMF train at 100 Oe field intensity that chirps linearly from 1 to 10 MHz, the volumetric heat dissipation produced over each 2π phase change of the AMF oscillation is estimated to increase from 0.15 to 1.1 μJ/cm^3 within the millisecond duration of the chirping of AMF.
Conclusions: The heat dissipations upon SPION ($\sim$1 mg/ml iron-weight concentration) by a 1 μs bursting of 100 Oe AMF at 10 MHz and a 1 ms train of 100 Oe AMF that chirps linearly from 1 to 10 MHz were estimated to determine the potential of thermal-acoustic wave generation. Although thermoacoustic wave generation from MNPs by time- or frequency-domain AMF applications is predicted, the experimental generation of such a wave remains challenging. © *2013 American Association of Physicists in Medicine*. [http://dx.doi.org/10.1118/1.4804056]

Key words: thermoacoustic imaging, alternating magnetic field, magnetic nanoparticle, superparamagnetic iron oxide, hyperthermia

I. INTRODUCTION

The heating effect of magnetic nanoparticles (MNPs), such as ferrofluids, when subjected to steady alternating magnetic field (AMF), has been known for many decades and implemented in various applications for industrial and medical purposes.[1,2] Under an AMF the MNPs undergo relaxation processes including hysteresis,[3] Brownian relaxation,[4] and Néel relaxation.[5] As the size of MNP reaches the superparamagnetic domain, Brownian relaxation and Néel relaxation become the increasingly dominant factors in the heat dissipation process.[6] Highly efficient heating of MNPs

using steady AMF, aided by localized or systematic targeting of MNPs to a disease site by conjugating MNPs with a ligand of biomarkers, has significantly mobilized the paradigm of hyperthermia for cancer treatment[7] and motivated developments of thermally sensitive payload release.[8]

In nearly all therapeutic applications of MNPs that utilize AMF to induce heat as the vehicle of treatment, the AMF is applied continuously over a duration that typically lasts a few tens of minutes. In some studies of thermally triggered drug release the AMF has been applied at a subsequent, long-pulse mode. For instance, NP-encapsulated liposome was subjected to five subsequent AMF pulses, each lasting 5 min with a 1-min equilibration interval between consecutive pulses.[9] Within each of these minutes-long pulses the AMF at a frequency of kHz level operates effectively as steady-state, i.e., the amplitude and frequency of AMF are fixed over a time-scale that is substantially (several orders) longer than the period of AMF oscillation.

In terms of the mechanism of AMF-induced heating of MNPs, most studies have adopted Rosensweig's model[10] that established the specific heat dissipation based on the Brownian and Néel relaxation characteristics of MNPs at a field intensity much lower than that causing saturated magnetization. Rosensweig's model justified a strong dependence of the heating efficacy upon the frequency of AMF for a given MNP size-domain. For a monodispersed superparamagnetic iron oxide nanoparticle (SPION), the model-predicted AMF frequency at which the maximum heat dissipation is produced is usually at or above 1 MHz. However, in most studies involving AMF-mediated heating of MNP, the AMF frequencies generally were between 100 and 500 KHz, and the field intensities were in the range from 50 to 300 Oe.[11] The diversity of the AMF parameters reported in existing studies was in part due to the custom-development of most AMF devices; however, it also represents a lack of consensus on the safety protocol regarding the product of the field intensity and frequency of AMF.[12]

It is noticed that the end result of MNP relaxation under AMF, specifically the conversion of the electromagnetic energy to heat, is not different from that of light being absorbed by chromophores such as hemoglobin and melanin, and microwaves being absorbed by dielectric tissue constituents, such as ion and water. As is well known, when the absorption of light or microwave varies rapidly, by either pulsing or amplitude modulation of the energy irradiation, the time-varying heat dissipation results in transient thermoelastic expansion that in turn induces acoustic wave—a mechanism broadly referred to as thermoacoustics. Thermoacoustic wave generation by light irradiation is specified as photoacoustics that has undergone galvanizing developments in the recent decade for some ground-breaking applications in microscopy[13] and small animal tomography.[14] Thermoacoustic wave generation by microwave irradiation has also been applied extensively in the form of microwave-induced thermoacoustic tomography.[15–17]

This study proposes a potentially new method of thermoacoustic wave generation—a mechanism referred to as "magnetothermoacoustics" as it employs the known heating effect of AMF-mediation of MNPs in thermoacoustic wave generation. To induce thermoacoustic wave generation, the AMF-mediation of MNPs must result in rapidly time-varying heat dissipation. Time-varying AMF-mediated heating of MNPs can be achieved by either a time-domain or a frequency-domain AMF configuration. The time-domain AMF configuration refers to applying AMF in a bursting mode and within each burst the AMF remains steady-state, resulting in the heating of MNPs to be established and removed instantly following the duty cycle of the bursting of AMF. A magnetic field intensity that does not oscillate within a burst of the field (but could vary within the burst) is simply a pulsatile magnetic field, which has been applied to magnetoacoustic modulation of MNPs for ultrasound imaging,[18,19] magnetomotive optical coherence tomography,[20] magnetoacoustic tomography with magnetic induction (MAT-MI) (Ref. 21) and magnetoacoustic tomography of MNPs.[22,23] In all these approaches, however, whether or not the acoustic signal is to be generated, the effect of the pulsatile magnetic field upon MNPs is a translational mechanical force imposed by the spatial gradient of the magnetic field, not necessarily the conversion of the magnetic field energy into heat. The proposed magnetothermoacoustic wave generation by applying time-domain AMF upon MNPs is through the magnetic relaxation loss that converts magnetic field energy to heat, which is mechanistically different from the dielectric loss of microwave energy in microwave-induced thermoacoustics, one study of which employed MNPs to enhance the contrast.[24] The frequency-domain AMF configuration refers to applying AMF continuously at constant amplitude but with frequency modulation (i.e., chirped). With a frequency-domain AMF, the heating of MNP varies following the cycle of the frequency modulation of AMF as a result of the strong frequency dependence of heat dissipation.

Section II implements Rosensweig's model in an alternative form to describe the heat dissipated by MNPs within one complete cycle (i.e., a 2π phase change) of the AMF intensity oscillation. Section II then expresses the heat dissipation of MNPs within a short bursting duration of AMF that contains integer numbers of complete cycles of AMF intensity oscillation, as well as the heat dissipated by MNPs within each 2π phase change of a linearly frequency chirped AMF. Section III describes experimental developments leading to measurements of the heating characteristics of a SPION matrix in a steady-state AMF at various frequencies between 88.8 kHz and 1.105 MHz. The measured initial rates of the temperature-rise were modeled by Rosensweig's theory, and projected to a 10 MHz AMF frequency. The projection was necessary to evaluate the potential for clinically relevant imaging, as a 1.55 mm axial resolution of acoustic detection requires the bursting of AMF to be not longer than 1 μs, and within 1 μs a 10 MHz AMF could have 10 complete cycles of field oscillation to dissipate the heat for thermoacoustic wave generation. Section IV estimates the volumetric heat dissipation from the tested SPION matrix when exposed to a 1-μs burst of AMF at 10 MHz frequency and at 100 Oe field intensity. Section IV also estimates the time-resolved heat dissipation of the tested SPION matrix when exposed to a 1-ms long train of AMF at 100 Oe field intensity whose frequency chirps linearly from 1

to 10 MHz. These estimations should indicate the likelihood of time-domain or frequency-domain magnetothermoacoustics.

II. THEORY

In 2002, Rosensweig developed an analytical model of heat dissipation by MNPs in a liquid matrix when exposed to AMF.[10] That model by default assumed a continuous-wave (CW) or steady-state AMF, i.e., the magnetic field intensity alternates at a fixed frequency and constant amplitude, and expressed the generated heat by volumetric power dissipation—the *volumetric heat accumulated over one second*—and it remains constant for a CW AMF over the course of magnetic field application. In the proposed time-domain magnetothermoacoustics, the AMF is to be applied at a short duration of microsecond scale that may allow the magnetic field to oscillate only a limited number of complete cycles. To quantify the total heat dissipation over the duration that the AMF is actively applied (i.e., the bursting duration), one can simply multiply the heat generated over a single cycle of the AMF oscillation with the total number of cycles (assuming integer numbers for convenience) contained in the duration of the AMF burst. In the proposed frequency-domain magnetothermoacoustics, as the AMF is to be applied continuously but the AMF frequency changes, the heat dissipation imposed has to be quantified for each individual cycle of the AMF field oscillation.

To facilitate the quantifications of the heat dissipation by MNPs in time- and frequency-domain AMF configurations, this study expresses Rosensweig's original model in an alternative form to represent the *volumetric heat* dissipation *over a 2π phase change of a steady-state AMF*. The result is used as the base formula to analyze the heat dissipation of MNPs accumulated over the bursting duration of an AMF in time-domain configuration, and to justify the time-varying heat dissipation of MNPs over individual cycles of a frequency-chirped AMF. Notice that the relation between a heat-dissipation and the initial acoustic pressure of thermally induced acoustic wave has been established,[13–17] under the condition of thermal and acoustic confinement. Therefore, an estimation of the heat dissipation of MNPs when exposed to a time- or frequency-domain AMF of practical utility could indicate the feasibility of magnetothermoacoustics.

II.A. Heat deposition by MNPs over a 2π phase change of a steady-state AMF

We adapt Rosensweig's model[10] to derive the heat dissipation by MNPs over a 2π phase change of a steady-state AMF. Assuming a constant density system, the first law of thermodynamics governs that

$$\frac{dU}{dt} = \frac{dQ}{dt} + \frac{dW}{dt}, \tag{1}$$

where U (unit: J) is the internal energy, Q (unit: J) is the heat added, and W (unit: J) is the magnetic work done on the system. The differential magnetic work by a collinear magnetic field is $dW = \vec{H} \bullet d\vec{B} = H \cdot dB$, where $\vec{H}$ (unit: A m^{-1} or $4\pi \times 10^{-3}$ Oe) is the magnetic field intensity and $\vec{B}$ (unit: T or V s m^{-2}) is the magnetic induction. As $B = \mu_0(H + M)$, where M (unit: A m^{-1}) is the magnetization and $\mu_0 = 4\pi \times 10^{-7}$ (unit: V s A^{-1} m^{-1}) is the permeability of free space, the differential internal energy for an adiabatic process, i.e., $\partial Q = 0$, becomes

$$\frac{dU}{dt} = \mu_0 H \cdot \left(\frac{dH}{dt} + \frac{dM}{dt}\right). \tag{2}$$

Denoting the dimension-less complex magnetic susceptibility of MNPs as $\chi = \chi' - i\chi''$, the real part of the susceptibility χ' and the imaginary part of the susceptibility χ'' under a time-varying magnetic field with an instant angular frequency ω become, respectively,

$$\begin{cases} \chi'(\omega) = \chi_0 \dfrac{1}{1 + [\omega\tau_R]^2} \\ \chi''(\omega) = \chi_0 \dfrac{\omega\tau_R}{1 + [\omega\tau_R]^2} \end{cases}, \tag{3}$$

where τ_R (unit: s) is the relaxation time, and χ_0 is the equilibrium susceptibility which can be calculated from the following expressions:

$$\chi_0 = \chi_i \frac{3}{\xi}\left(\coth\xi - \frac{1}{\xi}\right), \tag{4}$$

where

$$\chi_i = \frac{\mu_0 \phi M_d^2 V_M}{3k_B T_{\text{emp}}}, \tag{5}$$

$$\xi = \frac{\mu_0 M_d H_0 V_M}{k_B T_{\text{emp}}}, \tag{6}$$

where ϕ (dimensionless) is the volume fraction of the MNP solid in the host liquid matrix, M_d (unit: A m^{-1}) is the domain magnetization of MNP, V_M (unit: m^3) is the magnetic volume of MNP, H_0 is the amplitude of the magnetic field intensity, $k_B = 1.38 \times 10^{-23}$ (unit: m^2 kg s^{-2} K^{-1}) is the Boltzmann constant, and T_{emp} (unit: K) is the temperature. If the MNP in a liquid matrix is monodispersed in the superparamagnetic-size domain, the relaxation time τ_R is to be dominated by Néel and Brownian relaxations as[3,10]

$$\frac{1}{\tau_R} = \frac{1}{\tau_N} + \frac{1}{\tau_B}. \tag{7}$$

The Néel relaxation time τ_N in Eq. (7) is[5,10]

$$\tau_N = \frac{\sqrt{\pi}}{2}\tau_0 \frac{\exp\left(\dfrac{\kappa \cdot V_M}{k_B T_{\text{emp}}}\right)}{\sqrt{\dfrac{\kappa \cdot V_M}{k_B T_{\text{emp}}}}} \quad \tau_0 \sim 10^{-9}\ \text{s}, \tag{8}$$

where κ (unit: J m^{-3}) is the anisotropy energy density, and τ_0 is a nanosecond-scale characteristic time. The Brownian relaxation time τ_B in Eq. (7) is[4,10]

$$\tau_B = \frac{3\eta \cdot V_H}{k_B T_{\text{emp}}}, \tag{9}$$

where V_H (unit: m^3) is the hydrodynamic volume of MNP, and η (unit: N s m^{-2}) is the viscosity coefficient of the matric fluid.

A steady-state or CW AMF is represented by

$$H(t) = H_0 \cos(\omega_0 t) = \Re[H_0 \exp(i\omega_0 t)] \tag{10}$$

under which the MNP magnetization is

$$\begin{aligned} M(t) &= \Re[\chi \cdot H_0 \exp(i\omega_0 t)] \\ &= H_0[\chi' \cdot \cos(\omega_0 t) + \chi'' \cdot \sin(\omega_0 t)]. \end{aligned} \tag{11}$$

Then Eq. (2) becomes

$$\begin{aligned} \frac{dU}{dt} &= \frac{1}{2}\mu_0\omega_0 H_0^2[-(1+\chi') \cdot \sin(2\omega_0 t) \\ &\quad + \chi'' \cdot \cos(2\omega_0 t) + \chi'']. \end{aligned} \tag{12}$$

Integrating Eq. (12) over a full cycle or 2π phase change of AMF oscillation results in the *heat dissipation per unit volume* (unit: J m^{-3}) *over a duration of* $\Delta t_{2\pi} = 2\pi/\omega_0$ as

$$\begin{aligned} \Delta q_{2\pi} &= \int_{t-\Delta t_{2\pi}}^{t} U' dt = \mu_0 \pi H_0^2 \chi'' \\ &= \mu_0 \pi H_0^2 \chi_0 \frac{\omega_0 \tau_R}{1 + [\omega_0 \cdot \tau_R]^2}. \end{aligned} \tag{13}$$

The thermal energy deposited per unit volume per unit time, i.e., the *volumetric power dissipation* (unit: W m^{-3}), is then

$$q_{\mathrm{CW}} = \Delta q_{2\pi} \cdot \frac{1}{\Delta t_{2\pi}} = \frac{\mu_0 \chi_0}{2\tau_R} \frac{[\omega_0 \cdot \tau_R]^2}{1 + [\omega_0 \cdot \tau_R]^2} H_0^2, \tag{14}$$

where the subscript "CW" denotes "continuous-wave." Accordingly, for a MNP-liquid system that has a mass-density ρ (unit: kg m^{-3}) the *specific-loss-power* (SLP) (unit: W kg^{-1}) is

$$\mathrm{SLP}_{\mathrm{CW}} = \frac{q_{\mathrm{CW}}}{\rho} = \frac{\mu_0 \chi_0}{2\rho\tau_R} \frac{[\omega_0 \cdot \tau_R]^2}{1 + [\omega_0 \cdot \tau_R]^2} H_0^2. \tag{15}$$

Under a CW AMF as illustrated in Fig. 1(a), the heat is continuously deposited by MNP at a constant rate as specified by Eq. (15), therefore no thermoacoustic wave is to be generated,[13] and the effect of this time-invariant heat dissipation is a steady rise of the local temperature for an adiabatic process. In practice, however, the MNP-liquid matrix transfers the heat to the ambient environment, so the temperature and volume of MNP-liquid matrix will rise and expand until a thermoequilibrium with the environment (i.e., the tissue) is reached. The initial rate of the temperature rise of the MNP-liquid system is defined as[10]

$$\left.\frac{dT_{\mathrm{emp}}}{dt}\right|_{t=0} = \frac{\mathrm{SLP}_{\mathrm{CW}}}{C_V} = \frac{\mu_0 \chi_0}{2\rho C_V \tau_R} \frac{[\omega_0 \cdot \tau_R]^2}{1 + [\omega_0 \cdot \tau_R]^2} H_0^2, \tag{16}$$

where C_V (unit: J kg^{-1} K^{-1}) is the specific heat of the MNP-liquid system at a constant volume. Equation (16) is frequently used to predict and experimentally deduce the SLP of MNPs when exposed to a steady-state AMF for studies of localized hyperthermia and controlled drug release.

II.B. Time-domain magneto thermoacoustics from MNPs exposed to a short bursting of AMF

By exposing MNPs to an AMF of a short duration, such as a microsecond burst within which the magnetic field intensity of AMF alternates at several MHz, the relaxation of MNP will be established abruptly as the AMF is turned on at the beginning of the bursting and removed instantaneously as the AMF is turned off at the end of the bursting. The abrupt onset and removal of the AMF will result in rapidly time-varying heat dissipation, as depicted in Fig. 1(b), which in turn could induce thermoacoustic wave generation.

In the following we analyze the heat dissipation from MNP when exposed to a short duration of AMF. From the derivation of Eq. (13), it is appreciated that the cumulative contribution of the real part of the magnetic susceptibility χ' to the internal energy of MNP over a 2π phase change of a steady-state AMF is zero. Therefore, as long as there are integer numbers of 2π phase change (or equivalently integer number of complete cycles of oscillation) of the magnetic field within the duration of applying the field, $\Delta q_{2\pi}$ of Eq. (13) still quantifies the heat dissipation per unit volume over each single 2π phase change of the AMF. Consequently multiplying $\Delta q_{2\pi}$ with the total number of complete cycles of magnetic field oscillation gives the total heat dissipation per unit volume that is accumulated over the duration of AMF application. In terms of the width of the bursting of AMF for imaging purposes, as the axial resolution of thermoacoustics

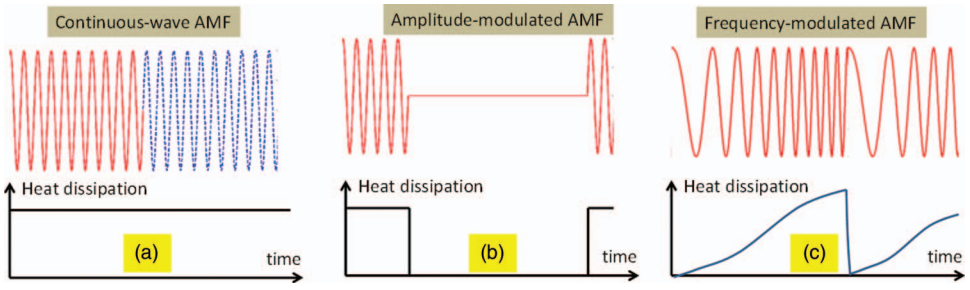

FIG. 1. Time-dependence of the heat dissipation from MNPs when exposed to AMF of different configurations. (a) A continuous-wave AMF with constant amplitude and frequency results in time-invariant heat dissipation, which will not induce thermoacoustic wave generation. (b) A burst of AMF with constant amplitude within the burst duration results in heat dissipation that is established when the AMF burst is on and removed when the AMF burst is off. (c) A train of AMF with constant amplitude but the frequency chirped results in heat dissipation that is varying according to the frequency of AMF. The configurations of both (b) and (c) are expected to induce thermoacoustic wave generation.

is limited by the temporal width of the irradiation pulse and the temporal width of the impulse response of the ultrasonic transducer,[25] a burst width of AMF less than 1 μs is necessary if the axial resolution of acoustic detection is to be better than 1.55 mm.[13] A pulse width of 1 μs is common to the microwave-irradiation in microwave-induced thermoacoustic tomography,[16,17,25] though much longer than the pulse width of light irradiation for photoacoustics.

We thus consider a simplest form of time-domain AMF, as illustrated in Fig. 1(b), that is to apply a short bursting of AMF at fixed frequency and fixed amplitude at a low duty cycle. This short bursting of AMF can be expressed as a "carrier" AMF being modulated by an envelope function of a pulse train. The envelope function, denoted by $\Omega(t)$, is written by using the Heaviside or unit-step function $u(t)$ as

$$\Omega(t) = \sum_{n=0}^{\infty}[u(t - n \cdot \Delta T_{\mathrm{TD}}) - u(t - \Delta t_{\mathrm{ON}} - n \cdot \Delta T_{\mathrm{TD}})],$$
$$n = 1, 2, 3, \ldots, \tag{17}$$

where ΔT_{TD} is the period of the pulse train, the subscript "TD" denotes "time-domain," and Δt_{ON} is the width of each burst within which the AMF maintains fixed frequency and fixed amplitude. The time sequence $\Omega(t)$ of Eq. (17) basically specifies when a steady-state AMF is turned on or off, and it satisfies the following specific condition:

$$\Omega(t) = [\Omega(t)]^2, \tag{18}$$

without which Eq. (20) below should contain additional terms. The magnetic field of this time-domain AMF is then represented by

$$H_{\mathrm{TD}}(t) = H_0(t)\cos(\omega_0 t) = \Omega(t)[H_0\cos(\omega_0 t)]. \tag{19}$$

Based on Eq. (13) the *volumetric heat dissipation* of MNPs at a position $\vec{r}'$ due to a pulse-enveloped time-domain AMF characterized by Eqs. (10), (17) and (18) is

$$\Delta q_{\mathrm{TD}}(\vec{r}', t) = \mu_0 \pi H_0^2 \chi_0(\vec{r}') \frac{\omega_0 \tau_R(\vec{r}')}{1 + [\omega_0 \tau_R(\vec{r}')]^2} \frac{\Delta t_{\mathrm{ON}}}{\Delta t_{2\pi}}. \tag{20}$$

Following the time-varying cycle of $\Omega(t)$, the heat dissipation $\Delta q_{\mathrm{TD}}(\vec{r}', t)$ of MNP that varies rapidly over time will give rise to a thermoacoustic wave, at the falling edges of $\Omega(t)$. Notice that Eq. (20) is derived by assuming that the steady heat dissipation is established at an infinitesimally short moment after the steady-state AMF is turned on and removed immediately after the steady-state AMF is turned off, according to Eq. (17). Such assumption ignores the effect of high frequency components of the AMF that arise at the moments of the rapid establishment or removal of the AMF field, and those high-frequency components will complicate the signal spectrum of thermoacoustic wave in a practical measurement.

The thermally generated acoustic pressure $p_{\mathrm{TD}}(\vec{r}, t)$ at a specific location $\vec{r}$ satisfies the following equation that has been well documented in photo- or microwave-induced thermoacoustics:[13,17,26]

$$\nabla^2 p_{\mathrm{TD}}(\vec{r}, t) - \frac{1}{c_a}\frac{\partial^2}{\partial t^2} p_{\mathrm{TD}}(\vec{r}, t) = -\frac{\beta}{C_p}\frac{\partial}{\partial t}\Delta q_{\mathrm{TD}}(\vec{r}, t), \tag{21}$$

where c_a (unit: m s^{-1}) is the speed of acoustic wave in tissue, β (unit: K^{-1}) is the isobaric volume thermal expansion coefficient, and C_p (unit: J kg^{-1} K^{-1}) is the specific heat at a constant pressure. The general solution of the acoustic pressure that originates from the source of thermoacoustic wave at $\vec{r}'$ and reaches a point transducer at $\vec{r}$ in an unbounded medium is[13]

$$p_{\mathrm{TD}}(\vec{r}, t) = \frac{\beta}{4\pi C_p}\int_V \frac{1}{|\vec{r} - \vec{r}'|}\frac{\partial}{\partial t}\Delta q_{\mathrm{TD}} \times \left(\vec{r}', t - \frac{|\vec{r} - \vec{r}'|}{c_a}\right) \cdot d^3\vec{r}'. \tag{22}$$

When the distance between the source and the measurement points, $l = |\vec{r} - \vec{r}'|$, is much greater than the dimension of the source, and the thermoacoustic source is approximated by a uniform distribution of MNPs in a volume $V(\vec{r}')$, Eq. (22) can be simplified to

$$p_{\mathrm{TD}}(\vec{r}, t) = \frac{\beta}{4\pi C_p}\frac{V(\vec{r}')}{l}\frac{\partial}{\partial t}\Delta q_{\mathrm{TD}}\left(\vec{r}', t - \frac{l}{c_a}\right). \tag{23}$$

Equation (21) states that heat dissipation at a constant rate does not induce thermoacoustic wave, which is what occurs when CW AMF of fixed frequency and amplitude is applied upon MNPs. However, thermoacoustic wave generation could have occurred at the instants of setting off the CW AMF in hyperthermia and particularly in the studies of triggered drug release[9] wherein the minute-long AMF trains were repetitively applied.

II.C. Frequency-domain magneto thermoacoustics from MNPs exposed to linearly frequency-chirped AMF

We analyze the heat dissipation of MNPs exposed to a frequency-domain AMF that has fixed amplitude H_0 with a varying frequency. The simplest form of a frequency-domain AMF may be one that has a linearly modulated or chirped frequency, as shown in Fig. 1(c), which has an instantaneous angular frequency of

$$\omega(t) = \omega_{\mathrm{st}} + bt, \tag{24}$$

where ω_{st} is the starting frequency and b is the rate of frequency sweeping. The instantaneous field strength of this linearly frequency chirped AMF is

$$H_{\mathrm{FD}}(t) = H_0\cos[\omega t] = H_0\cos[(\omega_{\mathrm{st}} + bt)t], \tag{25}$$

where the subscript "FD" denotes "frequency-domain." The resulted magnetization is

$$M(t) = \Re[\chi \cdot H_0\exp(i\omega t)] = H_0[\chi'(\omega)\cdot\cos(\omega t) + \chi''(\omega)\cdot\sin(\omega t)]. \tag{26}$$

Substituting Eqs. (25) and (26) to Eq. (2) leads to

$$\frac{dU}{dt} = \frac{1}{2}\mu_0 H_0^2\left[(1 + \cos(2\omega t))\frac{d\chi'}{dt} + \sin(2\omega t)\frac{d\chi''}{dt} + \chi''(1 + \cos(2\omega t))\frac{d(\omega t)}{dt} - (1 + \chi')\sin(2\omega t)\frac{d(\omega t)}{dt}\right]. \tag{27}$$

We denote a "positive-zero-crossing" phase as the instant when the magnetic field strength is zero and the next value is positive, i.e., the instant crossing the abscissas upwardly. Then integrating Eq. (27) over a 2π phase change of the AMF starting at a "positive-zero-crossing" phase is equivalent to integrating Eq. (27) from an earlier phase of $\omega_0 t_0 = (n-1)*2\pi$, where n is a positive integer, to the current phase of $\omega t = n*2\pi$. If we denote $\Delta t_{2\pi}$ as the time taken for the phase of AMF to change 2π from the earlier "positive-zero-crossing" instant to the current "positive-zero-crossing" instant, we have

$$\omega_0 t_0 = \omega_0(t - \Delta t_{2\pi}) = \omega t - 2\pi \quad \text{or}$$

$$\Delta t_{2\pi} = \frac{2\pi}{\omega_0} - \frac{(\omega - \omega_0)}{\omega_0} t. \tag{28}$$

Integration of Eq. (27) over the $\Delta t_{2\pi}$ duration results in the following instantaneous volumetric heat dissipation:

$$\Delta q_{\mathrm{FD}}(t) = \int_{t-\Delta t_{2\pi}}^{t} U' dt = \mu_0 \pi H_0^2 \chi_0 \frac{\omega \tau_R}{1 + [\omega \cdot \tau_R]^2} - \frac{5}{4} \mu_0 H_0^2 \chi_0 \left[\frac{1}{1 + (\omega_0 \cdot \tau_R)^2} - \frac{1}{1 + (\omega \cdot \tau_R)^2} \right]. \tag{29}$$

Apparently Eq. (29) becomes Eq. (13) for CW AMF if the frequency modulation is turned off [i.e., $b = 0$ in Eq. (24)]. With the frequency modulation, $\Delta q_{2\pi}(t)$ represented by Eq. (29) changes periodically following the cycle of the frequency chirping, and the instantaneous $\Delta q_{2\pi}(t)$ is strongly dependent upon the AMF frequency according to the magnetic susceptibility term at a given magnetic field intensity. Notice that the second term in Eq. (29) that involves the differentiation between the earlier "positive-zero-crossing" phase and the current "positive-zero-crossing" phase will modify the proportionality of the heat dissipation to the first term in Eq. (29). Collectively, the time-varying heat dissipation upon MNPs due to frequency-chirped AMF mediation will give rise to a thermoacoustic wave.

We denote $\Delta q_{\mathrm{FD}}(\vec{r}, t)$ as the volumetric heat dissipation at a position $\vec{r}$ at an instant t produced by a frequency chirped AMF represented by Eq. (25), and the Fourier transform of $\Delta q_{\mathrm{FD}}(\vec{r}, t)$ as $\Delta \tilde{Q}_{\mathrm{FD}}(\vec{r}, \tilde{\omega})$. Accordingly, the acoustic pressure excited by $\Delta q_{\mathrm{FD}}(\vec{r}, t)$ is represented by $p_{\mathrm{FD}}(\vec{r}, t)$, and the Fourier transform of $p_{\mathrm{FD}}(\vec{r}, t)$ is denoted as $\tilde{P}_{\mathrm{FD}}(\vec{r}, \tilde{\omega})$. The propagation of $\tilde{P}_{\mathrm{FD}}(\vec{r}, \tilde{\omega})$ is then expressed by the following Fourier-domain wave equation:

$$\nabla^2 \tilde{P}_{\mathrm{FD}}(\vec{r}, \tilde{\omega}) + \frac{(\tilde{\omega})^2}{c_a} \tilde{P}_{\mathrm{FD}}(\vec{r}, \tilde{\omega}) = -\frac{i\tilde{\omega}\beta}{C_p} \Delta \tilde{Q}_{\mathrm{FD}}(\vec{r}, \tilde{\omega}). \tag{30}$$

The general solution of Eq. (30) for the acoustic pressure that reaches a transducer at $\vec{r}$ and originates from the source of thermoacoustic wave at $\vec{r}'$ in an unbounded medium is[27]

$$\tilde{P}_{\mathrm{FD}}(\vec{r}, \tilde{\omega}) = -\frac{i\tilde{\omega}\beta}{4\pi C_p} \int_V \frac{\exp[ik|\vec{r} - \vec{r}'|]}{|\vec{r} - \vec{r}'|} \Delta \tilde{Q}_{\mathrm{FD}}(\vec{r}, \tilde{\omega}) d^3\vec{r}'. \tag{31}$$

If the distance between the source and the measurement points, $l = |\vec{r} - \vec{r}'|$, is much greater than the dimension of the source and the thermoacoustic source is approximated by a uniform distribution of MNPs in a volume $V(\vec{r}')$, Eq. (31) is simplified to

$$\tilde{P}_{\mathrm{FD}}(\vec{r}, \tilde{\omega}) = -\frac{i\tilde{\omega}\beta}{4\pi C_p} \frac{V(\vec{r}')}{l} \Delta \tilde{Q}_{\mathrm{FD}}(\vec{r}, \tilde{\omega}) \exp[ik|\vec{r} - \vec{r}'|]. \tag{32}$$

Therefore, the acoustic wave intercepted by a point ultrasound transducer at $\vec{r}$ that locates at a distance of $l = |\vec{r} - \vec{r}'|$ from the source of thermoacoustic wave can be written as

$$P_{\mathrm{FD}}(\vec{r}, t) = \frac{\beta}{4\pi C_p} \frac{V(\vec{r}')}{l} \frac{\partial}{\partial t} \Delta q_{\mathrm{FD}} \left(\vec{r}', t - \frac{l}{c_a} \right) \times \exp\left\{ i \left[\tilde{\omega} \left(t - \frac{l}{c_a} \right) + \theta_a \right] \right\}, \tag{33}$$

where θ_a is a phase constant related to thermoelastic conversion.[27] Equation (33) states that an AMF of fixed frequency (at constant intensity as is CW AMF), as it gives rise to a constant Δq upon the mediation of MNPs, does not induce thermoacoustic wave.

III. ESTIMATION OF THE HEAT DISSIPATION FROM SPION BY TIME-DOMAIN OR FREQUENCY-DOMAIN AMF BASED ON EXPERIMENTALLY MEASURED HEATING CHARACTERISTICS

We estimate the heat dissipation of a SPION sample in a time-domain or frequency-domain configuration of AMF at a field intensity of 100 Oe that may be of practical utility. The estimation is rendered by using experimentally measured heating characteristics of a SPION sample at a 0.8 mg/ml iron-weight concentration when exposed to CW AMF at various frequencies ranging from 88.8 kHz to 1.105 MHz and the field intensity normalized at 100 Oe. The experimentally measured heating characteristics are modeled by Eq. (16), and the modeling is then projected to 10 MHz in order to evaluate the potential of magnetothermal heat dissipation by ten complete cycles of AMF oscillation within a 1-μs burst. The 1-μs width of the AMF burst is what is necessary to achieving a 1.55 mm axial resolution of acoustic detection. As a qualitative evaluation we also estimated the heat dissipation due to a chromophore at different depths in a typical biological tissue when subjected to near-infrared light of a surface irradiation fluence limited for nontherapeutic use according to American National Standards Institute (ANSI). Specifically, the evaluation is for a volumetric heat dissipation by a 100 mJ/cm^2 near-infrared surface illumination upon a chromophore that has onefold or tenfolds (by endogenous chromophore such as hemoglobin) of absorption contrast over the background biological medium that has a reduced scattering coefficient of

10 cm^{-1} and an absorption coefficient of 0.1 cm^{-1}. In addition, the time-varying volumetric heat dissipation by the SPION sample exposed to an AMF train that chirps linearly from 1 to 10 MHz over a 1 ms duration is estimated.

III.A. A continuous wave AMF system for SPION based hyperthermia

A continuous wave AMF system has been developed for therapeutic evaluation of hyperthermia induced by SPION.[28] The AMF device, of which the schematic is shown in Fig. 2(a) and the photograph of the coil part is shown in Fig. 2(b), has an applicator coil of 5 cm long and 5 cm in diameter, with a center clearance of 4 cm in diameter allowing the head of a rat to be placed. The single-layer solenoid consisted of a few turns of 1/4 in. hollow copper tubing around a Teflon substrate. The hollow copper tubing was terminated through Teflon tubing to a water chiller that regulated the circulation of deionized water at a preset temperature. A heavy-duty capacitor bank was placed in series with the AMF applicator coil to create an inductor–capacitor (LC) network that was driven at its resonant frequency. Sinusoidal RF signal from a function generator was amplified by a class B RF power amplifier (T&C Power Conversion, Rochester, NY) that was capable of delivering 500 W to a 50 Ω load within a FWHM bandwidth of 80–800 kHz. Custom-designed tapping terminals were mounted to the solenoid coil for adjusting the coupling efficiency between the RF power amplifier and the coil-capacitor resonant circuit. By different combinations of the four capacitors, CW AMF with a frequency between 88.8 kHz and 1.102 MHz was obtained. Due to limited positioning of the tapping terminals, the coupling of the RF power to the coil was not optimal across all frequencies of choices, and the field strengths measured at the center region of the coil varied from 52 Oe (4.14 kA/m) to 220 Oe (17.5 kA/m) in the frequencies realized. The field strength was measured by placing a single turn pick-up coil of 1.27 cm in diameter inserted to the middle-section of the AMF coil and converting the induced frequency-proportional voltage. The temperature of the SPION sample was measured by an immerged fiber optical temperature sensor connected to a multichannel data monitor (FISO, Quebec, QC, Canada) through computer interface for continuous data acquisition.

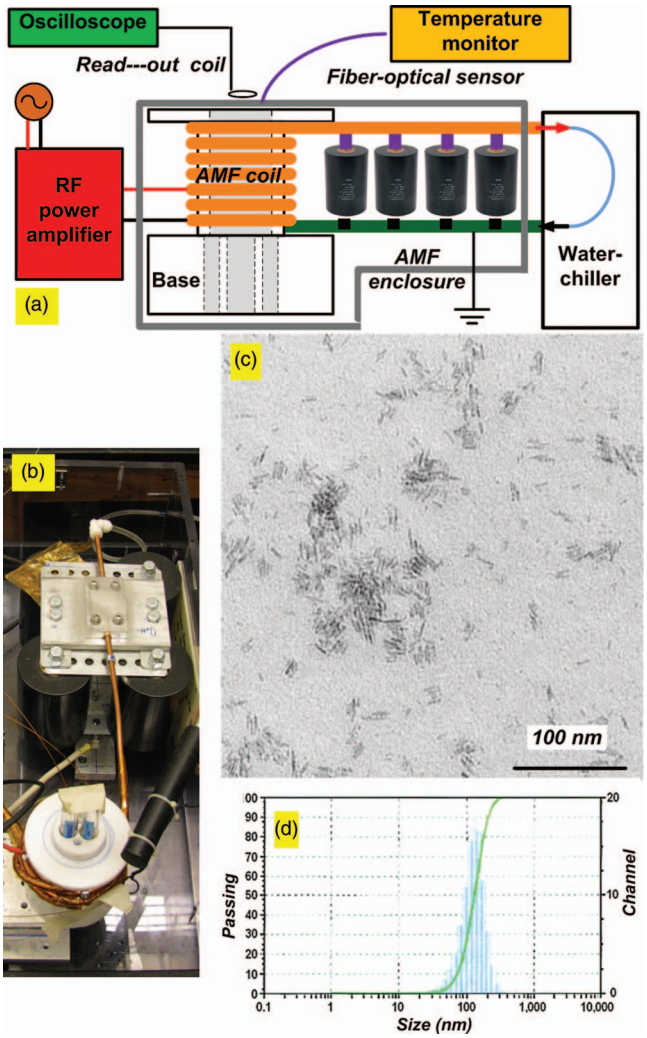

FIG. 2. The AMF setup and the SPION. (a) Schematic diagram of the AMF setup consisting of a water-chilled copper-coil, a bank of heavy-duty capacitors, a signal generator, a RF power amplifier, an AMF read-out coil, and a fiber-optic temperature sensor module. (b) Photograph of the AMF coil shown at the bottom that is coiled by copper tubing of 1/4 in. diameter and connected to the capacitor bank shown at the top. (c) Transmission electron microscopy of the SPION cores averaging from 9 to 10 nm (larger sizes are aggregates). (d) Dynamic light scattering (Nanotrak) particle size analysis of the CLIO nanoparticles (~120 nm).

III.B. The SPION sample

A dextran based cross-linked iron oxide (magnetite) (CLIO) nanoparticle[29,30] was used as the SPION sample for measurement of initial temperature rise under steady-state AMF. Transmission electron microscopy shown in Fig. 2(c) was used to establish the core-size of the dextran coated nanoparticles, which were found to have an elongated shape, with an average length of 9–10 nm and clustered in 20–60 nm aggregates. Dynamic light scattering (Nanotrak particle size analysis) shown in Fig. 2(d) was used to establish the hydrodynamic size of the nanoparticles formed in the carrier fluid, which were found to have an average size of ~120 nm. The SPION sample used for the benchtop testing had an iron-weight concentration of 0.8 mg/ml. The weight concentration of the SPION in the host medium was measured experimentally as 0.64% (an average obtained from duplicates), which corresponds to 0.0946% volume fraction of the SPION solids in the liquid matrix based on the mass densities of the magnetite and the carrier fluid as specified in Table I.

III.C. Initial rate of temperature rise of the SPION matrix under CW AMF

A 20-ml vial containing 5 ml of 0.8 mg/ml SPIONs was placed in the AMF coil for measuring the heating of the SPION matrix under CW AMF. The initial rate of temperature rise in degree/second was calculated based on the initial slope of the temperature change after the onset of AMF.

TABLE I. Material-specific parameters (Refs. 10 and 31) used for simulating the heat dissipation of SPION.

Symbol	Parameter specification	Value	Unit
c_a	Speed of sound in tissue	1550	m s^{-1}
C_V	Specific heat of carrier fluid	2080	J kg^{-1} K^{-1}
H	Magnetic field strength	7.96	kA m^{-1}
M_S	Saturation magnetization	446	kA m^{-1}
T_{emp}	Thermodynamic temperature	298	K
V_M	Magnetic volume	Corresponding to a diameter of 9.5 nm	m^3
V_H	Hydrodynamic volume	Corresponding to a diameter of 120 nm	m^3
η	Viscosity coefficient	0.00235	N s m^{-2}
κ	Anisotropy energy density of Fe_3O_4	23 (the smallest value used by Ref. 10. The higher the value, the higher the heat dissipation.)	J m^{-3}
ρ	Mass density of Fe_3O_4	5180	kg m^{-3}
ρ	Mass density of carrier fluid	765	kg m^{-3}

Temperature was continuously monitored over the duration of AMF application that lasted between several minutes to 40 min, depending upon the actual heating rate and the interested range of temperature measurement. Because the AMF intensities were different across the frequencies realized, the temperature rise was normalized to an AMF field intensity of 100 Oe (7.96 kA/m), based on the dependence of heat dissipation upon the square of AMF field intensity. The experimentally measured initial rates of temperature rise were than compared to the model-prediction by Eq. (16) using the material and dimensional parameters detailed in Table I. The results are shown in Fig. 3(a). The heating characteristics when projected to 20 MHz using Eq. (16) is shown in Fig. 3(b) (it was evaluated but not illustrated here that, as the frequency reaches 40 MHz and above, the curve levels off and eventually flattens). The heat dissipation expressed as temperature change per time (i.e., power) is shown to rise monotonically with the frequency over the range shown, and a 10 times of increase of frequency from 1 to 10 MHz results in approximately 84 times of increase of the heat dissipation.

III.D. Estimation of the heat dissipation by 0.8 mg/ml SPION under a 1-μs burst of 10 MHz AMF and a 1-ms train of AMF with the frequency chirping from 1 to 10 MHz

At 10 MHz, a 1-μs burst of AMF contains ten complete cycles. If a 1-μs burst of AMF at 10 MHz and 100 Oe is applied to the same 0.8 mg/ml SPION matrix used for the experimental measurement, the volumetric heat dissipation based on Eq. (20) is 7.7 μJ/cm^3. This value corresponds to the horizontal line shown in Fig. 4(a). As the tissue attenuation to time-varying magnetic field of 10 MHz is negligible[21] comparing to the near-infrared light, the AMF induced heat dissipation from SPION can be assumed depth-invariant. However, the photo-induced heat dissipation is strongly dependent upon the depth from the irradiation. In regards to the potential of thermoacoustic wave generation, it is imperative to compare the 7.7 μJ/cm^3 heat dissipation estimated for SPION under a time-domain AMF against the heat dissipation by a chromophore in tissue under a surface light illumination as strong as 100 mJ/cm^2. For a typical biological tissue that has a reduced scattering coefficient of $\mu'_s = 10\,\text{cm}^{-1}$ and an absorption coefficient of $\mu_a = 0.1\,\text{cm}^{-1}$, the fluence in tissue in the diffusion region due to a surface fluence Ψ_0 reduces quickly versus the depth r at a rate that is not smaller than the following one well-known for an unbounded medium:

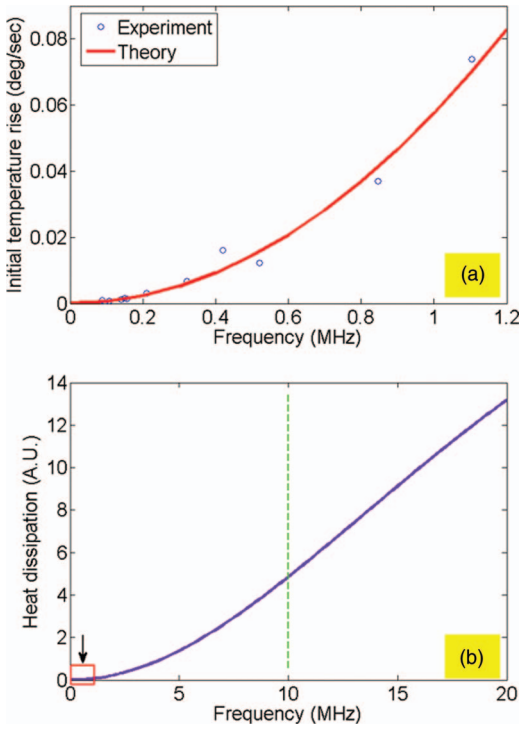

FIG. 3. (a) Circles represent the measurement of the initial rate of temperature rise (deg/s) of the 0.8 mg/ml SPION sample at a number of AMF frequencies and normalized at the AMF field intensity of 100 Oe. The solid line is the theoretical fitting based on Eq. (16) using the parameters in Table I. (b) Projecting the theoretical fitting of (a) to 20 MHz AMF frequency leads to the line shown. The portion of the line within the rectangle marked by the arrow corresponds to the solid line shown in (a). A 10 times of frequency increase from 1 to 10 MHz results in approximately 84 times of increase of the heat dissipation.

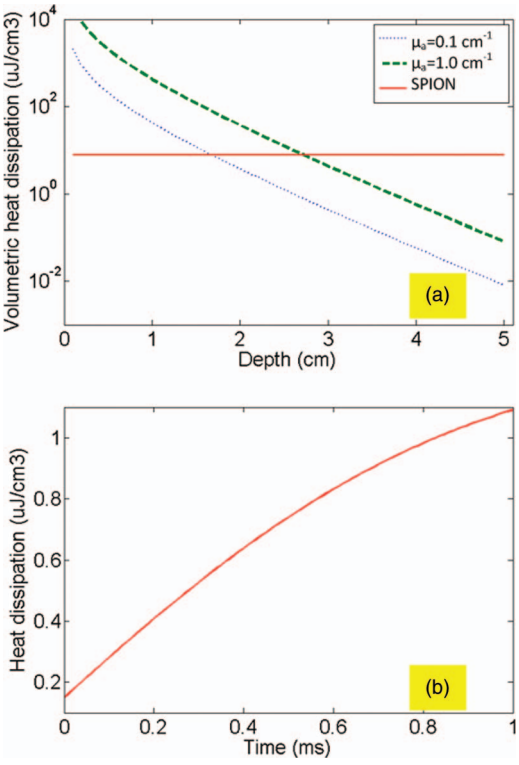

FIG. 4. (a) The horizontal solid line corresponds to 7.7 μJ/cm^3 volumetric heat dissipation by 0.8 mg/ml SPION accumulated over a 1-μs burst of 10 MHz 100 Oe AMF. The dashed and dotted lines are the estimated volumetric heat dissipation upon a chromophore over the depth of tissue generated by a surface light illumination of 100 mJ/cm^2. The background biological tissue is assumed to have a reduced scattering coefficient of 10 cm^{-1} and an absorption coefficient of 0.1 cm^{-1}. The heat dissipation is calculated by assuming that light propagates in the tissue of given properties before reaching the chromophore by which the light fluence is absorbed to become heat. The dotted line represents the chromophore of $\mu_a^{\text{chro}} = 0.1\,\text{cm}^{-1}$, i.e., the same absorption coefficient as the background medium. The dashed line represents the chromophore of $\mu_a^{\text{chro}} = 1\,\text{cm}^{-1}$, a tenfolds of absorption contrast over the background medium. (b) The heat dissipation by 0.8 mg/ml SPION during a 1-ms train of 100 Oe AMF whose frequency is linearly chirped from 1 to 10 MHz.

$$\Psi_r = \Psi_0 \frac{3(\mu_a + \mu_s')}{4\pi} \frac{\exp(-\sqrt{3\mu_a(\mu_a + \mu_s')}r)}{r}. \tag{34}$$

The heat deposited by a chromophore of absorption coefficient μ_a^{chro} is then

$$\Delta q(r, \mu_a^{\text{chro}}) = \mu_a^{\text{chro}} \Psi_0. \tag{35}$$

At a surface irradiation fluence of $\Psi_0 = 100$ mJ/cm^2, the heat deposited by a chromophore of $\mu_a^{\text{chro}} = 0.1\,\text{cm}^{-1}$ or $\mu_a^{\text{chro}} = 1\,\text{cm}^{-1}$ versus the depth of the chromophore in the biological tissue of $\mu'_s = 10\,\text{cm}^{-1}$ and $\mu_a = 0.1\,\text{cm}^{-1}$, according to Eqs. (34) and (35), is shown as the dashed or dotted curve in Fig. 4(a). The case of $\mu_a^{\text{chro}} = 0.1\,\text{cm}^{-1}$ corresponds to the heat dissipation in the biological tissue with no specific chromophore, whereas the case of $\mu_a^{\text{chro}} = 1\,\text{cm}^{-1}$ corresponds to the heat dissipation by a chromophore that has tenfolds of absorption contrast over the background tissue. Figure 4(a) shows that the predicted volumetric heat dissipation from the 0.8 mg/ml SPION matrix when exposed to 1 μs of AMF at 10 MHz and 100 Oe is comparable to the heat produced at 1.75 cm depth in a typical biological tissue under 100 mJ/cm^2 surface irradiation, and to the heat produced at 2.75 cm depth by a chromophore of 10 times of absorption contrast over the background biological tissue under the same amount of surface illumination. In comparison, Fig. 4(b) shows the estimated heat dissipation by the 0.8 mg/ml SPION matrix when exposed to a 1-ms train of 100 Oe AMF with the frequency chirping linearly from 1 to 10 MHz. The 1 ms duration is comparable to the duration of frequency-chirped amplitude modulation in the frequency-domain photoacoustics.[26] The heat dissipation of Fig. 4(b) is shown to increase monotonically from 0.15 to 1.1 μJ/cm^3 over the 1 ms duration of AMF frequency-chirping.

IV. DISCUSSION

In this study we proposed an alternative mechanism of thermoacoustics by utilizing the heating effect of MNPs under AMF as a result of magnetic relaxation as the source of thermoacoustic wave generation. The proposed magnetothermoacoustics may be useful to tracing MNP for therapeutic delivery, in a theranostic approach that could in principle use the same set of magnetic applicator for both imaging and therapeutic activation of the MNPs.

We estimated the heat from a 0.8 mg/ml SPION matrix after applying a 1-μs burst of 10 MHz 100 Oe AMF. It should be noticed that, the 0.8 mg/ml SPION matrix used for the model-computation is estimated to be 16 times of the safe dosing of SPION in plasma, 50 μg/ml, which corresponds to 5 mg/kg body-weight of SPION,[31,32] 50 kg body weight and 5000 ml blood. By targeting SPION with a specific biomarker, it may be feasible to enhance the site-specific delivery of the SPION multiple fold of that of the plasma concentration.[33] The volumetric heat dissipation over the 1-μs burst-width of AMF upon the 0.8 mg/ml SPION matrix seems comparable to the heat produced by a chromophore of an absorption coefficient of 1 cm^{-1} (or 0.1 cm^{-1}) at a depth of less than 3 cm (or 2 cm) in a typical biological tissue when a surface illumination as strong as 100 mJ/cm^2 is applied. However, the volumetric power dissipation by the predicted 1-μs burst AMF will likely be several orders smaller than what can be achieved by the typical nanosecond pulsed light irradiation in photoacoustics, resulting in an acoustic-signal intensity that is potentially several orders smaller than that obtained by nanosecond pulsed light irradiation.[34] It is therefore expected that the thermoacoustic signal generated from a site-specific SPION concentration at a tissue depth of several centimeters by applying a time-domain AMF of practical utility may be more challenging to detect than the photoacoustic signal produced at that depth by a maximum surface illumination used for time-domain photoacoustics. Additionally, at high frequency AMF field (~30 MHz), nonspecific heating[35] could reduce the expected thermoacoustic signal contrast of the site-specific SPION distribution.

The acoustic signal level acquired in frequency-domain photoacoustics is reported several orders smaller than that in time-domain photoacoustics[27] under similar irradiation and

depth conditions. It should be noticed that Eq. (29) represents the volumetric heat dissipation accumulated over an individual cycle of AMF oscillation and evaluated at the ending-point of that individual cycle. Therefore, it is in fact a discrete-representation of the volumetric heat dissipation and should not be considered as the instant volumetric power dissipation. Accordingly, the volumetric heat dissipation shown in Fig. 4(b) is evaluated at a discrete time corresponding to the "positive-zero-crossing" point of an individual cycle of AMF oscillation when it chirps linearly from 1 to 10 MHz and accumulated over that single cycle. So the heat dissipation values of 0.15–1.1 μJ/cm^3 in Fig. 4(b) are comparable in scale to the heat dissipation over only one cycle of AMF in Fig. 4(a), i.e., 0.77 μJ/cm^3, which is 1/10 of the 7.7 μJ/cm^3 heat dissipation accumulated over a total of ten cycles of AMF oscillation. The 1.1 μJ/cm^3 accumulated over one cycle of 10 MHz frequency-domain AMF is even greater than the 0.77 μJ/cm^3 accumulated over one cycle of 10 MHz time-domain AMF. This is related to the second term in Eq. (29), as it differentiates between the earlier "positive-zero-crossing" phase and the current "positive-zero-crossing" phase. As a result the gradient of the frequency-dependence of the heat-dissipation will contribute to the overall heat-dissipation in frequency-domain AMF configuration. However, it is the temporal gradient of the volumetric heat dissipation accounts for the magnitude of the acoustic signal as identified by Eqs. (23) and (33). Consequently, even though the volumetric heat dissipation accumulated over individual cycle of the frequency-domain AMF may be comparable to the volumetric heat dissipation accumulated over any one cycle of the time-domain AMF, in the specified time-domain AMF configuration a heat dissipation change of 7.7 μJ/cm^3 occurs within a 1 μs time-scale, whereas in the specified frequency-domain AMF configuration a heat dissipation change of less than 1 μJ/cm^3 occurs within a 1 ms time-scale. Therefore, it could be expected that the acoustic wave generated by frequency-domain magnetothermoacoustics will also be several orders smaller than that by time-domain magnetothermoacoustics, making it even more challenging to be detected.

Although it is expected that the acoustic signal to be produced by either time-domain or frequency-domain magnetothermoacoustics can be received by a hydrophone or an ultrasound transducer by synchronizing the acoustic measurement with the excitation cycle of AMF, there are more technical challenges to demonstrate magnetothermoacoustics. Using the AMF system shown in Fig. 2 as an example, based on the previous analysis, it would be necessary to operate the AMF at 10 MHz or a higher frequency to have sufficient heat dissipation upon the SPION to produce acoustic signal that may be detectable by a highly sensitive ultrasound transducer. As the AMF coil is networked with the capacitor bank, the AMF operates at the resonant frequency $f = 1/(2\pi\sqrt{LC})$, where L is the inductance of the AMF coil and C is the total capacitance of the capacitor bank. Therefore, a tenfolds increase of the resonance frequency from 1 to 10 MHz requires a 100 folds reduction of the capacitance, if the AMF coil remains. As the smallest capacitance of the heavy-duty capacitors used for the system shown in Fig. 2 was 0.004 μF, reaching a 10 MHz AMF frequency would require using capacitors of 0.00004 μF, at which capacitance it is difficult to find heavy-duty models with the current rating sufficient to producing the AMF intensity using the coil shown. Alternatively, the AMF coil has only a small number of turns, leaving not much room to reduce the number of turns to reduce the inductance, and any reduction in the number of turns will reduce the AMF field generated at a given current rating that would reduce the heat dissipation.

Even though the AMF-coil-capacitor network may be operated at 10 MHz or a higher frequency with the field intensity comparable to that produced by the system at 1 MHz as shown in Fig. 2, there are additional issues to consider. In terms of the frequency-domain AMF operation, it is necessary to have relatively uniform impedance matching of the AMF coil-network with the RF amplifier over the bandwidth of frequency chirping, which conflicts with the resonance configuration of the AMF coil-capacitor network. In terms of the time-domain AMF operation, although the AMF during the active excitation could operate at a fixed frequency of 10 MHz of interest, the AMF-coil-capacitor network must accommodate AMF operation at much higher frequency components, in order to maintain a sharp falling-edge of the amplitude envelope during the turning-off of the AMF in order to reach strong temporal gradient of the heat-dissipation. This again challenges the resonance configuration of the AMF-coil-capacitor network, let alone that the RF amplifier available for the system in Fig. 2 has a limited bandwidth of only up to 800 KHz. It is therefore anticipated that a broad-band matching between a RF amplifier and an AMF coil is necessary, and as such magnetothermoacoustics may be difficult to demonstrate using an AMF coil configured in a resonance network.

Regardless of the AMF configuration, the detection of the acoustic signal from MNPs will likely be interfered by the signals due to other metallic materials within the oscillating magnetic field. Electromagnetic interference is not an issue for photoacoustics; however, it will need to be negotiated in microwave-induced thermoacoustics by appropriate gating techniques. As such, the acoustic detection methods implemented in microwave-induced thermoacoustics[36] may be directly applicable to magnetothermoacoustics. A fiber-optical interferometry based sensor may be more robust for acoustic detection in magnetothermoacoustics.[37]

The theoretical modeling of the experimentally measured heating characteristics has been performed based on the simplest monodispersive model. A polydispersive model will certainly improve the estimation accuracy, if the core-size-distribution of the SPION can be precisely measured. The analysis in this study also treats thermal-acoustic wave generation due to only the temporal change of AMF, but the AMF has been assumed to be spatially homogenous, i.e., at a given time, the field strength is assumed uniform throughout the imaging domain. Consequently a spatially resolved magnetothermoacoustic measurement is to be associated in this case with only the specific concentration of the SPION. In practice, however, the spatial heterogeneity of AMF is inevitable and significant for coil of certain shape. The solenoid

coil commonly used for AMF generates a relatively uniform field only in the middle-section of the coil, whereas a Helmholtz type coil[38] applies a uniform magnetic field in a much greater area. The unavoidable spatial heterogeneity of the magnetic field then contributes to the acoustic generation by way of the magnetic gradient induced translational force[23] $F(\vec{r}) \propto \nabla \left[B(\vec{r})\right]^2$ upon MNPs, which modifies[23] the Eq. (21) of the time-domain magnetothermoacoustics to

$$\nabla^2 p_{\mathrm{TD}}(\vec{r},t) - \frac{1}{c_a}\frac{\partial^2}{\partial t^2} p_{\mathrm{TD}}(\vec{r},t) = -\frac{\beta}{C_p}\frac{\partial}{\partial t}\Delta q_{\mathrm{TD}}(\vec{r},t) + \nabla \bullet [F(\vec{r},t)] \quad (36)$$

and Eq. (30) of the frequency-domain magnetothermoacoustics to

$$\nabla^2 \tilde{P}_{\mathrm{FD}}(\vec{r},\tilde{\omega}) + \frac{(\tilde{\omega})^2}{c_a}\tilde{P}_{\mathrm{FD}}(\vec{r},\tilde{\omega}) = -\frac{i\tilde{\omega}\beta}{C_p}\Delta\tilde{Q}_{\mathrm{FD}}(\vec{r},\tilde{\omega}) + \nabla \bullet [\tilde{F}(\vec{r},\tilde{\omega})] \quad (37)$$

where $\tilde{F}(\vec{r},\tilde{\omega})$ is the Fourier-transform of $F(\vec{r},t)$ with respect to the time-argument.

V. CONCLUSIONS

The feasibility of thermoacoustic wave generation from MNP by applying a short burst of AMF or a frequency modulated AMF is proposed. As the relaxation of MNP under AMF is strongly dependent upon the amplitude and frequency of AMF, either a short bursting of AMF or a frequency chirped AMF will result in time-varying heat dissipation from MNP, which in turn has the potential to induce thermoacoustic wave generation. Based on experimentally measured heating characteristics of a 0.8 mg/ml SPION matrix under CW AMF, the heat dissipations of the SPION under a 1-μs burst of 10 MHz 100 Oe AMF and a 1-ms train of 100 Oe AMF with the frequency chirping linearly from 1 to 10 MHz are estimated. Thermoacoustic wave generation from MNPs of manageable *in vivo* concentrations by applying either a time-domain or frequency-domain AMF, however, is quite challenging.

ACKNOWLEDGMENT

This work was supported in part by a National Institutes of Health Grant No. 1 R21 CA136642-01A1.

[a]Author to whom correspondence should be addressed. Electronic mail: daqing.piao@okstate.edu

[1]J. Xie, J. Huang, X. Li, S. Sun, and X. Chen, "Iron oxide nanoparticle platform for biomedical applications," Curr. Med. Chem. **16**(10), 1278–1294 (2009) (Review).
[2]C. S. Kumar and F. Mohammad, "Magnetic nanomaterials for hyperthermia-based therapy and controlled drug delivery," Adv. Drug Delivery Rev. **63**(9), 789–808 (2011) (Review).
[3]R. Hergt, S. Dutz, and M. Röder, "Effects of size distribution on hysteresis losses of magnetic nanoparticles for hyperthermia," J. Phys. Condens. Matter **20**(38), 385214 (2008).
[4]J. Frenkel, *The Kinetic Theory of Liquids* (Dover Publications, New York, 1955).
[5]L. Néel, "Influence of thermal fluctuations on the magnetization of ferromagnetic small particles," C. R. Acad. Sci. **228**, 664–668 (1949).
[6]R. Hergt, S. Dutz, and M. Zeisberger, "Validity limits of the Néel relaxation model of magnetic nanoparticles for hyperthermia," Nanotechnology **21**(1), 015706 (2010).
[7]S. Balivada, R. S. Rachakatla, H. Wang, T. N. Samarakoon, R. K. Dani, M. Pyle, F. O. Kroh, B. Walker, X. Leaym, O. B. Koper, M. Tamura, V. Chikan, S. H. Bossmann, and D. L. Troyer, "A/C magnetic hyperthermia of melanoma mediated by iron(0)/iron oxide core/shell magnetic nanoparticles: A mouse study," BMC Cancer **10** (2010).
[8]C. Alexiou, R. Jurgons, C. Seliger, O. Brunke, H. Iro, and S. Odenbach, "Delivery of superparamagnetic nanoparticles for local chemotherapy after intraarterial infusion and magnetic drug targeting," Anticancer Res. **27**(4A), 2019–2022 (2007).
[9]E. Amstad, J. Kohlbrecher, E. Müller, T. Schweizer, M. Textor, and E. Reimhult, "Triggered release from liposomes through magnetic actuation of iron oxide nanoparticle containing membranes," Nano Lett. **11**(4), 1664–1670 (2011).
[10]R. E. Rosensweig, "Heating magnetic fluid with alternating magnetic fields," J. Magn. Magn. Mater. **252**, 370–374 (2002).
[11] A. C. Silva, T. R. Oliveira, J. B. Mamani, S. M. Malheiros, L. Malavolta, L. F. Pavon, T. T. Sibov, E. Amaro, Jr., A. Tannús, E. L. Vidoto, M. J. Martins, R. S. Santos, and L. F. Gamarra, "Application of hyperthermia induced by superparamagnetic iron oxide nanoparticles in glioma treatment," Int. J. Nanomed. **2011**(6), 591–603 (2011).
[12] I. Baker, Q. Zeng, W. Li, and C. R. Sullivan, "Heat deposition in iron oxide and iron nanoparticles for localized hyperthermia," J. Appl. Phys. **99**, 08H106 (2006).
[13]L. V. Wang, "Tutorial on photoacoustic microscopy and computed tomography," IEEE J. Sel. Top. Quantum Electron. **14**(1), 171–179 (2008).
[14]R. Su, S. A. Ermilov, A. V. Liopo, A. A. Oraevsky, "Three-dimensional optoacoustic imaging as a new noninvasive technique to study long-term biodistribution of optical contrast agents in small animal models," J. Biomed. Opt. **17**(10), 101506 (2012).
[15]T. Bowen, "Radiation-induced thermoacoustic soft tissue imaging," *1981 Ultrasonics Symposium* (IEEE, Piscataway, NJ, 1981), pp. 817–822.
[16]R. A. Kruger, K. K. Kopecky, A. M. Aisen, D. R. Reinecke, G. A. Kruger, and W. L. Kiser, Jr., "Thermoacoustic CT with radio waves: A medical imaging paradigm," Radiology **211**(1), 275–278 (1999).
[17]L. Nie, D. Xing, Q. Zhou, D. Yang, and H. Guo, "Microwave-induced thermoacoustic scanning CT for high-contrast and noninvasive breast cancer imaging," Med. Phys. **35**(9), 4026–4032 (2008).
[18]T. E. Milner, M. D. Feldman, C. Condit, and J. H. Oh, "Magneto-motive ultrasound detection of magnetic nanoparticles," U.S. patent application 20090043198 (12 February 2009).
[19] M. Mehrmohammadi, J. Oh, S. R. Aglyamov, A. B. Karpiouk, and S. Y. Emelianov, "Pulsed magneto-acoustic imaging," Conf. Proc. IEEE Eng. Med. Biol. Soc. **2009**, 4771–4774.
[20]A. L. Oldenburg, J. R. Gunther, and S. A. Boppart, "Imaging magnetically labeled cells with magnetomotive optical coherence tomography," Opt. Lett. **30**(7), 747–749 (2005).
[21]Y. Xu and B. He, "Magnetoacoustic tomography with magnetic induction (MAT-MI)," Phys. Med. Biol. **50**(21), 5175–5187 (2005).
[22]I. Steinberg, M. Ben-David, and I. Gannot, "A new method for tumor detection using induced acoustic waves from tagged magnetic nanoparticles," Nanomedicine **8**(5), 569–579 (2012).
[23]G. Hu and B. He, "Magnetoacoustic imaging of magnetic iron oxide nanoparticles embedded in biological tissues with microsecond magnetic stimulation," Appl. Phys. Lett. **100**(1), 013704-1–013704-3 (2012).
[24]L. Nie, Z. Ou, S. Yang, and D. Xing, "Thermoacoustic molecular tomography with magnetic nanoparticle contrast agents for targeted tumor detection," Med. Phys. **37**(8), 4193–4200 (2010).
[25]G. Ku and L. V. Wang, "Scanning microwave-induced thermoacoustic tomography: Signal, resolution, and contrast," Med. Phys. **28**(1), 4–10 (2001).
[26]L. Yao, G. Guo, and H. Jiang, "Quantitative microwave-induced thermoacoustic tomography," Med. Phys. **37**(7), 3752–3759 (2010).
[27]S. Telenkov, A. Mandelis, B. Lashkari, and M. Forcht, "Frequency-domain photothermoacoustics: Alternative imaging modality of biological tissues," J. Appl. Phys. **105**, 102029 (2009).

[28]D. Piao, K. Le, D. Saunders, N. Smith, J. Goddard, D. Figueroa, J. S. Krasinski, and R. A. Towner, "Development of a vertically and horizontally applicable multi-frequency alternating-magnetic-field device for hyperthermia of glioma in rodent model using iron oxide based nanoparticles," *Biomedical Optics and 3-D Imaging, OSA Optics and Photonics Congress*, 29 April–2 May 2012, Miami, Florida (Paper BSu3A.2).

[29]R. A. Towner, N. Smith, Y. Asano, T. He, S. Doblas, D. Saunders, R. Silasi-Mansat, F. Lupu, and C. E. Seeney, "Molecular magnetic resonance imaging approaches used to aid in the understanding of angiogenesis in vivo: Implications for tissue engineering," Tissue Eng. Part A **16**(2), 357–364 (2010).

[30]R. A. Towner, N. Smith, Y. Asano, S. Doblas, D. Saunders, R. Silasi-Mansat, and F. Lupu, "Molecular magnetic resonance imaging approaches used to aid in the understanding of the tissue regeneration marker Met in vivo: Implications for tissue engineering," Tissue Eng Part A **16**(2), 365–371 (2010).

[31]S. Purushotham and R. V. Ramanujan, "Modeling the performance of magnetic nanoparticles in multimodal cancer therapy," J. Appl. Phys. **107**, 114701 (2010).

[32]P. L. Apopa, Y. Qian, R. Shao, N. L. Guo, D. Schwegler-Berry, M. Pacurari, D. Porter, X. Shi, V. Vallyathan, V. Castranova, and D. C. Flynn, "Iron oxide nanoparticles induce human microvascular endothelial cell permeability through reactive oxygen species production and microtubule remodeling," Part Fibre Toxicol. **6** (2009).

[33]F. M. Kievit, Z. R. Stephen, O. Veiseh, H. Arami, T. Wang, V. P. Lai, J. O. Park, R. G. Ellenbogen, M. L. Disis, and M. Zhang, "Targeting of primary breast cancers and metastases in a transgenic mouse model using rationally designed multifunctional SPIONs," ACS Nano **6**(3), 2591–2601 (2012).

[34]C. Lou, S. Yang, Z. Ji, Q. Chen, and D. Xing, "Ultrashort microwave-induced thermoacoustic imaging: A breakthrough in excitation efficiency and spatial resolution," Phys. Rev. Lett. **109**(21), 218101 (2012).

[35]A. Cervadoro, C. Giverso, R. Pande, S. Sarangi, L. Preziosi, J. Wosik, A. Brazdeikis, and P. Decuzzi, "Design maps for the hyperthermic treatment of tumors with superparamagnetic nanoparticles," PLoS One **8**(2), (2013).

[36]R. A. Kruger, D. R. Reinecke, and G. A. Kruger, "Thermoacoustic computed tomography—Technical considerations," Med. Phys. **26**(9), 1832–1837 (1999).

[37]Y. Wang, C. Li, and R. K. Wang, "Noncontact photoacoustic imaging achieved by using a low-coherence interferometer as the acoustic detector," Opt. Lett. **36**(20), 3975–3977 (2011).

[38]M. Hedayati, A. Attaluri, D. Bordelon, R. Goh, M. Armour, H. Zhou, C. Cornejo, M. Wabler, Y. Zhang, T. DeWeese, and R. Ivkov, "New iron-oxide particles for magnetic nanoparticle hyperthermia: An in-vitro and in-vivo pilot study," Proc. SPIE **8584**, 858404-1–858404-10 (2013).